Environmental Earth Sciences (2023) 82:547
https://doi.org/10.1007/s12665-023-11252-z

ORIGINAL ARTICLE

Microscopic mechanisms of shear strength variation in acid- and alkali-contaminated loess

Kuan Liu[1,2,3] · **Wanjun Ye**[2] · **Pengwei Long**[4]

Received: 13 June 2022 / Accepted: 24 October 2023 / Published online: 2 November 2023

Abstract

The effect of the attack by chemical contaminants on the microstructure of loess and the resultant changes in shear strength properties threaten the safety of engineering projects in Northwest (NW) China. The aim of this study was to investigate the microscopic mechanisms of the variation in shear strength of acid- and alkali-contaminated loess. Intact loess samples were immersed in acid and alkali solutions of various concentrations, and triaxial shear, scanning electron microscopy (SEM), and mercury intrusion porosimetry (MIP) measurements were then conducted to assess the effects of acid and alkali contamination on the shear strength and microstructure of loess. The results indicated that the shear properties (stress−strain behavior, failure strength and cohesion) of loess deteriorated under acid contamination but were improved under alkali contamination. The structural damage (particle fragmentation, cement dissolution, and pore expansion) in acid-contaminated loess intensified with increasing acid concentration. In contrast, structural improvement occurred in alkali-contaminated loess because new cementation balanced local damage and enhanced the degree of structural connection. In acid-contaminated loess, the diffuse double layer (DDL) thinned, the calcium carbonate content rapidly decreased, and the liquid limit (LL) and plastic limit (PL) declined, while in alkali-contaminated loess, these parameters were improved. A series of physicochemical reactions (mineral dissolution, ion exchange, and particle and pore structure adjustment) in the presence of acid and alkali contamination drove the observed structural variation in loess. This comprehensive effect resulted in either loess shear strength enhancement or reduction, depending on whether damage to the original structure or formation of a new structure dominated, respectively. These findings contribute to a deeper understanding of the response of intact loess under various hydrochemical conditions, which has important practical significance for elucidating the disaster mechanism of loess slopes and facilitating ecological environment protection in acid–alkali-polluted areas.

Keywords Contaminated soil · Shear strength · Microscopic mechanisms · Scanning electron microscopy · Mercury intrusion porosimetry

Introduction

Loess refers to a natural aeolian sediment with a unique structure (large pores and unconsolidated particles) and a complex composition (calcium salts and clay minerals); loess covers 10% of the land area on Earth (Liu and Ding 1998; Pécsi 1990; Rogers et al. 1994; Wang et al. 2022). In recent years, the economy in the loess regions of Northwest (NW) China has greatly increased, but the fragile ecological environment has suffered increasing contamination (Hu

✉ Kuan Liu
19104053006@stu.xust.edu.cn

Wanjun Ye
yewanjun@xust.edu.cn

Pengwei Long
longpengwei@nwepdi.com

[1] College of Geology and Environment, Xi'an University of Science and Technology, No. 58 Yanta Rd., Xi'an 710054, Shaanxi, China

[2] School of Architecture and Civil Engineering, Xi'an University of Science and Technology, Xi'an 710054, Shaanxi, China

[3] Post-Doctoral Research Station of Geological Resources and Geological Engineering, Xi'an University of Science and Technology, Xi'an 710054, Shaanxi, China

[4] Northwest Electric Power Design Institute Co., Ltd., China Power Engineering Consulting Group, Xi'an 710075, Shaanxi, China

et al. 2022; Li et al. 2019b, 2022; Lian et al. 2020b; Liu et al. 2021a; Ma et al. 2021; Nan et al. 2021b; Wang et al. 2022; Yan et al. 2021; Zhang et al. 2018b; Zhu et al. 2023). Since industrial and domestic sewage contains abundant sources of acid and alkali contamination, the engineering properties of natural loess considerably vary upon contamination, even resulting in the instability of building foundations.

However, the soil shear strength is a crucial parameter regarding the design of the foundation bearing capacity and evaluation of the slope stability. Thus, the change in the soil shear strength in various hydrochemical environments has attracted increasing attention among researchers (Abedi Koupai et al. 2020). The variation in the residual shear strength of weathered mudstone contaminated by sodium chloride (NaCl) solutions of various concentrations was investigated by Tiwari et al. (2005). They reported that the reason for the increase in the residual shear strength of mudstone after salt contamination was that a high concentration of salt ions in pore water caused notable thinning of the diffuse double layers (DDLs) of clay particles. Through ring-shear tests, Gratchev Ivan and Sassa (2013) reported that the residual shear strength of soil in the sliding zone decreased upon contamination with sulfuric acid (H_2SO_4), sodium hydroxide (NaOH), and NaCl solutions of different pH levels, and they proposed that this was related to a decrease in the soil plasticity index. Evidently, the above studies focused more on the residual shear strength to explain the triggering mechanism of landslides. The latest available data on the peak shear strength of soil aim to characterize the effects of organic and inorganic solutions on several clays, but the findings are inconsistent (Komine and Watanabe 2010; Spagnoli et al. 2012). For instance, the effects of three organic chemical solutions (glycerol, 1-propanol and acetone) on the peak shear strength of three graded soils (one silt and two clay soils) were evaluated by Ratnaweera and Meegoda (2006), who considered that the observed reduction in the shear strength of the two clay soils (low and high plasticity levels) occurred due to the deterioration in friction characteristics at the particle contact surface under the influence of the viscous solution. In contrast, the effect of solutions containing different contaminants (such as formamide, ethanol, acetic acid, heptane, and triethylamine) on the stress−strain behavior and shear strength of kaolinite was assessed by Anandarajah and Zhao (2000). They indicated that the soil shear strength was improved due to excessive consolidation (reduction in the double-repulsive force and enhancement in the van der Waals force). Moreover, the undrained shear properties (determined by a vane shear apparatus) of clays (kaolin and montmorillonite) contaminated by three chloride solutions of various pH values (0–10) were estimated by Spagnoli et al. (2012). They observed a notable growth in the shear strength at low (3) and high (8) pH values, but the liquid limit (LL) varied only slightly. Additionally, the shear strength properties of Kawasaki mud (containing montmorillonite) and Yurakucho saline soil (containing kaolinite) subjected to long-term acid contamination (H_2SO_4) were investigated by Gratchev and Towhata (2013). They observed that the shear strength of these two soils marginally increased when the pH of the pore fluid decreased to a value of 6. However, most of the above studies included kaolin, montmorillonite or bentonite. In regard to natural loess, research on this topic is lacking. Zhang et al. (2020) proposed a shear strength attenuation model for loess under the coupled conditions of acid (H_2SO_4) and alkali (NaOH) contamination and freeze−thaw cycles, but they did not explain the degradation mechanisms and neglected to examine the distinct structural features of loess.

Although the conclusions reported in the above studies are diverse, it has been consistently found that the effect of the hydrochemical environment on the shear strength of soil is related to the variation in the soil microstructure, ionic environment and plasticity (Alonso et al. 2013; Delage et al. 1996; Lian et al. 2021; Nan et al. 2021b; Tan et al. 2021; Wang et al. 2023; Wang and Siu 2006). This has motivated researchers to investigate the evolution of the microstructure, ionic composition and Atterberg limits of soils (Husein Malkawi et al. 1999). The chemical composition, Atterberg limits and microstructure of two types of residual soils (sedimentary and igneous) under long-term contamination (1–20 years) by acid rain (simulated by H_2SO_4 and nitric acid, HNO_3) were determined by Bakhshipour et al. (2016), who revealed the mechanisms underlying the evolution of the soil compressive strength and permeability. Furthermore, scanning electron microscopy (SEM) and X-ray diffraction (XRD) were employed by Chavali et al. (2017) to explain the mechanisms of the variation in one-dimensional swelling of three kaolin clays under NaOH contamination. Only a few studies have focused on loess contaminated by landfill leachate (Lu et al. 2018) or the effect of the change in the pore water salt concentration (Xu et al. 2020; Yu et al. 2019), while various aspects of acid and alkali contamination remain unclear. Sun et al. (2021) reported the shear strength of intact Xiashu loess contaminated by acid (H_2SO_4) and alkali (NaOH) solutions. They focused on the effect of the soil structure on the physicomechanical properties, thereby emphasizing the mineral composition and microaggregation. However, they ignored the critical ion exchange effect and did not determine a general microscopic mechanism. Numerous investigations have focused on various soil engineering characteristics and considered the effect of assorted chemical solutions. However, due to the structural particularity and compositional complexity of natural loess, many of its geotechnical characteristics require further investigation under the influence of notable industrial acid and alkali contamination. Notably, the potential microscopic mechanism of shear strength variation remains unclear.

In this study, triaxial shear tests and SEM and mercury intrusion porosimetry (MIP) experiments, in addition to chemical composition and Atterberg limit determination tests, were performed involving intact loess contaminated by hydrochloric acid (HCl) and NaOH solutions. Furthermore, the microscopic mechanisms of the observed variation in the shear strength of loess contaminated by acid and alkali solutions were explained. The results of this study could help engineers better understand the mechanical response of intact loess to different hydrochemical environments.

Materials and methods

Materials

The analyzed soil was retrieved from Ning County in Gansu Province (35° 27′ 58″ N, 107° 59′ 47″ E, as shown in Fig. 1), where industrial acid and alkali contamination of the water–soil system is common. With reference to the standard for geotechnical engineering exploration (ASTM 2014; MCPRC 2009), the loess specimens were obtained approximately 3.5–3.8 m below the ground surface to avoid the influences of vegetation and human activities on the inherent soil properties. The soil is grayish-yellow in color with a certain moisture level. According to reports on the loess strata in eastern Gansu (Ma et al. 2012; Wen and Yan 2014; Zhu et al. 2022), the soil is Late Pleistocene Q_3 loess. Referring to geotechnical test standards (ASTM 2011a; MWPRC 2019), the basic geotechnical and mineralogical properties of the sampled loess were determined, as summarized in Table 1. Although silt (0.063–0.002 mm) dominated the loess grain size distribution, the Atterberg limits fell within the range of lean clay on the plasticity chart. On the basis of the unified

Table 1 Geotechnical and mineralogical properties of the loess

Parameter	Value	Standard
Natural moisture content (%)	13.80	GB/T50123-2019
Dry density (g/cm^3)	1.41	
Specific gravity	2.72	
Atterberg limits		
Liquid limit (LL, %)	34	GB/T50123-2019
Plastic limit (PL, %)	18	
Plasticity index (PI, %)	16	
Grain size distribution		
Gravel (≥ 2 mm, %)	0	USCS (ASTM D2487-11)
Sand (2 mm–0.063, %)	3	
Silt (0.002 mm–0.063 mm, %)	75	
Clay (≤ 0.002 mm, %)	22	
Soil classification	CL	

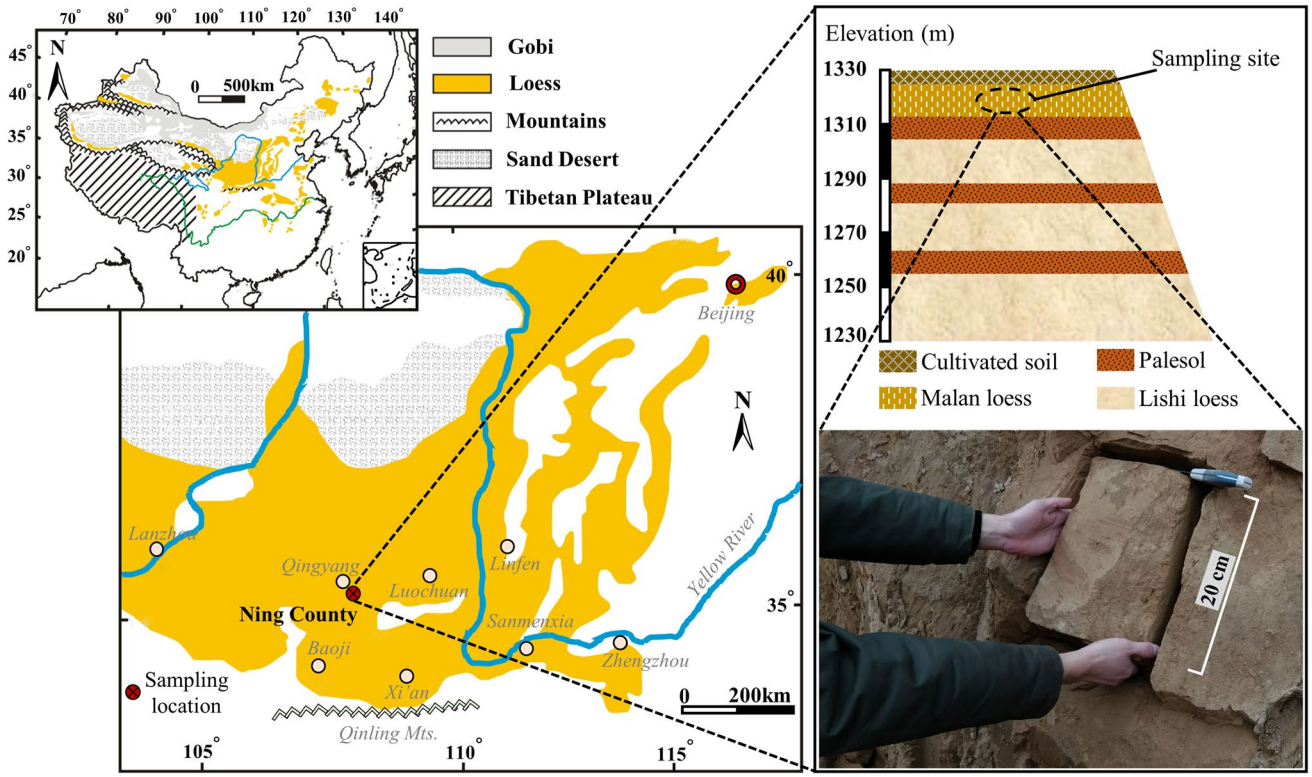

Fig. 1 Sampling site at Ning County, Gansu Province, China

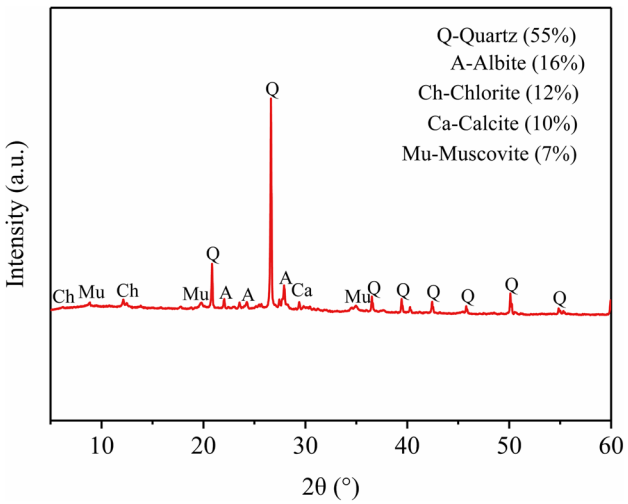

Fig. 2 XRD diffraction pattern of the loess

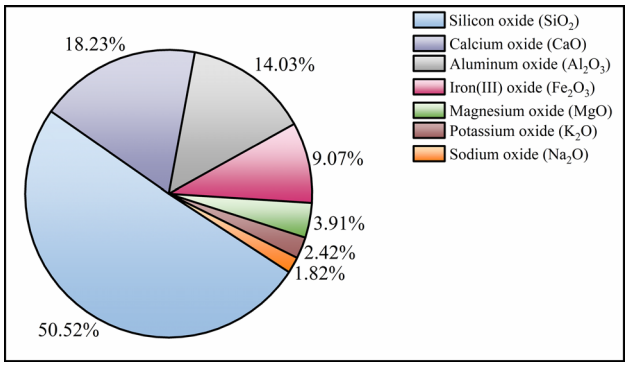

Fig. 3 Major chemical oxides present in the loess (unit: wt pct). Note: wt pct means weight percentage

soil classification system (ASTM 2011a), the tested loess was classified as clay of low plasticity (CL). Following the method described by Graham (1999), the composition of soil minerals was identified with an XRD instrument (XRD-7000S, Shimadzu), and the results are shown in Fig. 2. The results indicated that the mineral composition was dominated by quartz and albite with a small amount of chlorite. In addition, the average chemical composition of the soil was identified via X-ray fluorescence (XRF) analysis, and the results are shown in Fig. 3. Silica (SiO_2) is the most abundant in the analyzed soil (50.52%), followed by calcium carbonate ($CaCO_3$, 18.23%), and the total quantity of metal oxides (sesquioxide) was determined at 31.25%.

Contaminated sample preparation

The preparation of intact loess specimens contaminated by acid and alkali is shown in Fig. 4a. Intact soil specimens were prepared in accordance with guidelines of the Ministry of Water Resources of the People's Republic of China (MCPRC 2009). First, the intact soil was cut into cylindrical samples (diameter of 39.1 mm and height of 80 mm) and disk-shaped samples (diameter of 61.8 mm and height of 20 mm). Notably, the disk-shaped samples were directly obtained with a custom ring cutter constructed of Teflon material since the traditional metal ring cutter may affect subsequent tests. Acid- and alkali-contaminated samples were prepared via the immersion method (Sun et al. 2021; Zhang et al. 2018a). The pH level and ion concentration of 20 groups of surface water and groundwater samples obtained at various sampling sites were analyzed. The Cl^- content was much higher than the SO_4^{2-} content in the samples (more than 10 groups). Therefore, HCl and NaOH solutions were employed to simulate acid and alkali contamination, respectively. Based on these data and referring to previous studies (Sun et al. 2021; Xu et al. 2021; Zhang

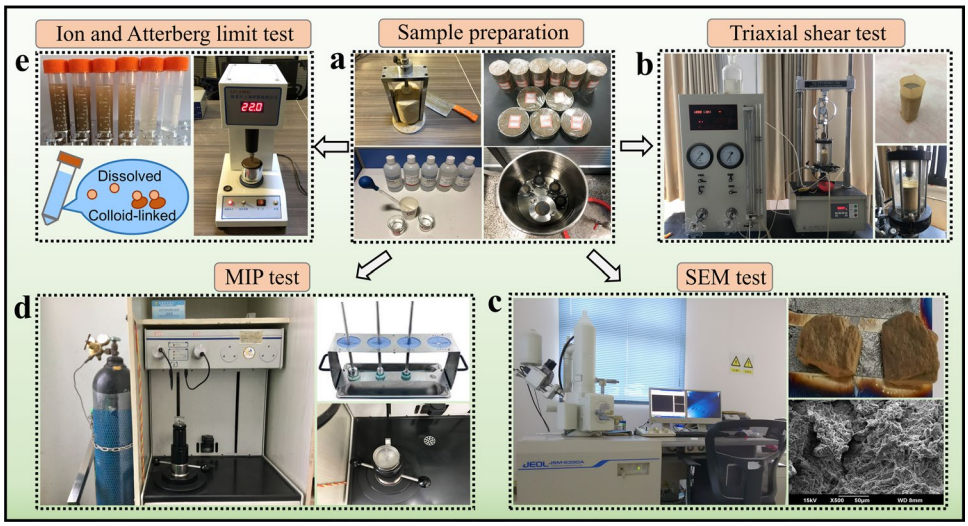

Fig. 4 General schematic diagram of the test scheme

et al. 2018b, 2020), the concentrations of the acid and alkali solutions were set to 0.5 mol/L (M), 1 M, 2 M and 3.5 M. The 2 M and 3.5 M solutions were employed to simulate environments with significant acid or alkali contamination (such as those affected by the leakage of acid and alkali materials stored in factories), and the 0.5 M solution was utilized to reproduce an environment with low acid or alkali contamination (such as the dilution effects of groundwater and rainfall on acid and alkali contamination). Moreover, the 1 M solution represents an environment with moderate acid and alkali contamination. For comparison purposes, deionized water was employed to simulate natural uncontaminated conditions, i.e., neutral pore fluid. Notably, the HCl solution was prepared by diluting 36.5% concentrated hydrochloric acid with water, and the NaOH solution was prepared by dissolving high-purity NaOH pellets in water.

The process of immersion in either an acid or alkali solution was conducted with reference to the capillary saturation method of the MWPRC (2019). This ensured that each sample was completely contaminated, the integrity satisfied follow-up tests, the metal saturator remained uncorroded, and the immersion method was slightly improved. In regard to the cylindrical samples, the entire length of the body was sequentially wrapped with a porous membrane and filter paper, after which filter paper and a permeable end plate were placed in sequence at both the top and bottom. The whole sample was fixed in a customized Teflon three-part mold, and three valves were finally tightened to secure the sample. Regarding the disk-shaped samples, a porous membrane, filter paper, and permeable end plate was placed in sequence at both the top and bottom, each of the four samples was stacked, and finally, a stacked saturator was employed for fixation purposes. Referring to previous studies (Sun et al. 2021; Zhang et al. 2018a, 2020), the tentative immersion time was set to 3, 4, 5 and 6 days. To confirm the homogeneity of the contaminated samples, after immersion, each sample was cut lengthwise to determine whether a hard core remained due to uneven infiltration. After multiple sets of tests, the ideal immersion time was determined as 5 days. When a sample was immersed in a given HCl solution, bubbles formed around the sample, while during immersion in a NaOH solution, little evidence of a reaction was observed. After the sample was disassembled and allowed to stand for a certain period, the sample immersed in the HCl solution had darkened with corrosion holes in some parts accompanied by a slightly pungent smell. However, the volume of the sample immersed in the NaOH solution slightly expanded, and white crystals were observed on the surface. After each sample was naturally dried (at approximately 25 °C, with a relative humidity of 50%), it was periodically weighed until the water content approached 16% (accuracy ± 0.2%) and then placed in a humidor (48 h) to attain an even moisture distribution.

Test program

Triaxial shear test

The consolidation time of the sediment samples was much longer than the construction period (the load application time) (Spagnoli et al. 2012). Four cylindrical samples immersed in either an HCl or NaOH solution of the same concentration were selected, and a triaxial apparatus (TSZ-3, Nanjing Soil Instrument Factory Co., Ltd.; as shown in Fig. 4b) was employed to perform consolidation undrained (CU) shear tests. First, the samples were saturated under a certain back pressure (300 kPa) before shearing (until the pore water pressure coefficient (B) was not less than 0.95). Then, the samples were consolidated in the triaxial chamber for approximately 24–48 h until 95% of the excess pore pressure had dissipated (Dai et al. 1999; Lian et al. 2020a). After consolidation, the confining pressure was maintained constant, the drain valve was closed, and shearing was started at a fixed shearing velocity of 0.033 mm/min (MWPRC 2019). The consolidated confining pressures applied in the tests were 50, 100, 200, and 400 kPa. During shearing, when the peak deviator stress was observed, shearing was continued until the axial strain increased by 3–5%. When no peak deviator stress was recorded (i.e., the stress exhibited no decrease tendency), shearing was continued until the axial strain reached 15–20% (MWPRC 2019). Following the approach described in the geotechnical testing standard (ASTM 2011b; MWPRC 2019) and the previous study on this topic (Eid et al. 2019; Lian et al. 2019), the stress of the specimen corresponding to the maximum deviator stress was adopted as the failure stress; when no maximum deviator stress was recorded, the deviator stress at 15% of the axial strain was considered the failure stress. To fully determine the trend, three sets of parallel tests were completed with each contaminated solution.

MIP and SEM tests

The microstructure of natural loess includes soil particles, pores, and cement. The soil particles and cement were observed via SEM, and the pores were analyzed via MIP (Liu et al. 2023; Nan et al. 2021a; Shen et al. 2022; Xu et al. 2023).

A completely air-dried disk-shaped sample (placed in a naturally ventilated location, 25 °C ± 0.5 °C, RH of 50%, 10 days) (Penumadu and Dean 2000) was carefully trimmed, and representative freshly fractured surface slices were selected to prepare SEM specimens (approximately 5 mm^3) (Li et al. 2019a; Ng et al. 2020b). The shooting surface (i.e., the freshly fractured surface) was sputtered with platinum by a sputter coater and then pasted onto the shooting platform. An SEM instrument (JEOL JSM-6390A) was employed to

obtain micrographs (100×, 3000×, and 8000×, where × denotes the magnification) of the soil samples (Fig. 4c).

Disk-shaped samples immersed in HCl or NaOH solutions of various concentrations were selected. After they were completely dried under natural conditions, the nearly cylindrical samples (approximately ϕ 10 mm × 10 mm) were trimmed along their center with a soil cutter. Prior to the MIP test, each sample was completely dehydrated via the freeze-drying method, namely, it was placed in the vacuum chamber of a freeze-dryer (for 48 h at – 60 °C) (Lian et al. 2022; Nan et al. 2021a), which effectively avoided any interference originating from its structure (Ng et al. 2019). After treatment, following the relevant ASTM (2018), the samples were moved into a dilatometer (5 cm^3 of solids), sealed, and then placed in the pressure chamber of a mercury porosimeter (AutoPore IV9510, Micromeritics) to perform tests for determining the pore characteristics (Fig. 4d). The above steps were repeated to analyze all the contaminated samples.

The pore diameter of a given soil sample is closely related to the mercury ingress volume corresponding to each pressure increment (Stoltz et al. 2012). Assuming that the loess pores are cylindrical channels, the pore diameter can be quantified with the Washburn (1921) equation:

$$d = \frac{-4T_s \cos\theta}{P} \tag{1}$$

where d is the pore entry diameter, P is the applied pressure, T_s is the surface tension of the fluid (at 0.485 N/m (Mitchell and Soga 2007)), and θ is the contact angle between the fluid and solid interface (at 140° (Romero 1999)). To estimate the evolution of the soil pore structure, the pore size density (PSD) function proposed by Juang and Holtz (1986) was introduced, which can be expressed as:

$$f(\lg d_i) = \frac{\Delta V_i}{\Delta(\lg d)} \tag{2}$$

where V is the injected mercury volume (i.e., the pore volume), d is the pore entry diameter, and i denotes a certain test pressure interval.

Chemical composition and Atterberg limits

The variation in the mechanical properties of contaminated soil is closely related to the change in its chemical composition and plasticity (Gajo and Maines 2007; Wang and Siu 2006). Determination of the chemical composition of loess mainly includes insoluble salts (calcium carbonate, $CaCO_3$) and pore water pH value. According to MCPRC (2009), the disk-shaped samples (previously immersed in the various solutions) were naturally dried, crushed and sieved (2-mm aperture), and an appropriate amount of deionized water was added. The samples were then shaken, aspirated, filtered and poured into centrifuge tubes (10 mL). According to the method described by Bufflap and Allen (1995), the leachate of each group of samples was extracted (at 3500 r/min, 40 min). The main cations (Na^+, Ca^{2+}, Mg^{2+}, K^+, Fe^{3+} and Al^{3+}) were determined via inductively coupled plasma−optical emission spectrometry (ICP−OES, Agilent 725 series), and Cl^- and SO_4^{2-} were identified with an ion chromatography instrument (IC-761 Metrohm), while CO_3^{2-} and HCO_3^-HCO-3 were measured via the neutralization titration method. The insoluble salt $CaCO_3$ was analyzed through gas (CO_2) volume measurement (MWPRC 2019). The pH value of the pore fluid at room temperature was measured with a pH meter. The evolution of the Atterberg limits was determined based on the LL and PL combined method. The above tests were repeated three to five times to reduce the random errors (Fig. 4e).

Results

Shear mechanical properties

Stress−strain behavior

Figure 5 shows the stress−strain curves of the samples after immersion in the HCl or NaOH solutions of various concentrations. After immersion in an HCl solution, the maximum deviator stress of each sample exhibited a decreasing trend under all confining pressures, and the reduction increased with increasing acid concentration. In contrast, the development of the stress−strain curves of the samples immersed in a NaOH solution was similar to that of the samples immersed in an HCl solution. However, the maximum deviatoric stress significantly increased with increasing alkali solution concentration. This was the opposite of the result obtained after immersion in an HCl solution. Comparing acid and alkali contamination showed that the effect of the confining pressure on the shape of the stress−strain curves should not be ignored. However, regarding the acid- and alkali-contaminated samples, the overall trend was consistent. They all demonstrated a transition from strain softening to ideal plasticity with increasing confining pressure, and they finally approached strain-hardening. Comparing Fig. 5e and i demonstrates that the effect of HCl and NaOH contamination on the shape of the soil stress−strain curve was negligible. Nevertheless, in general, HCl immersion imposed a deteriorating effect on the maximum deviator stress of loess, while NaOH immersion yielded a promoting effect.

Failure strength

The relationship between the failure strength and confining pressure of the contaminated samples is shown in Fig. 6. After the intact loess samples were immersed in the HCl

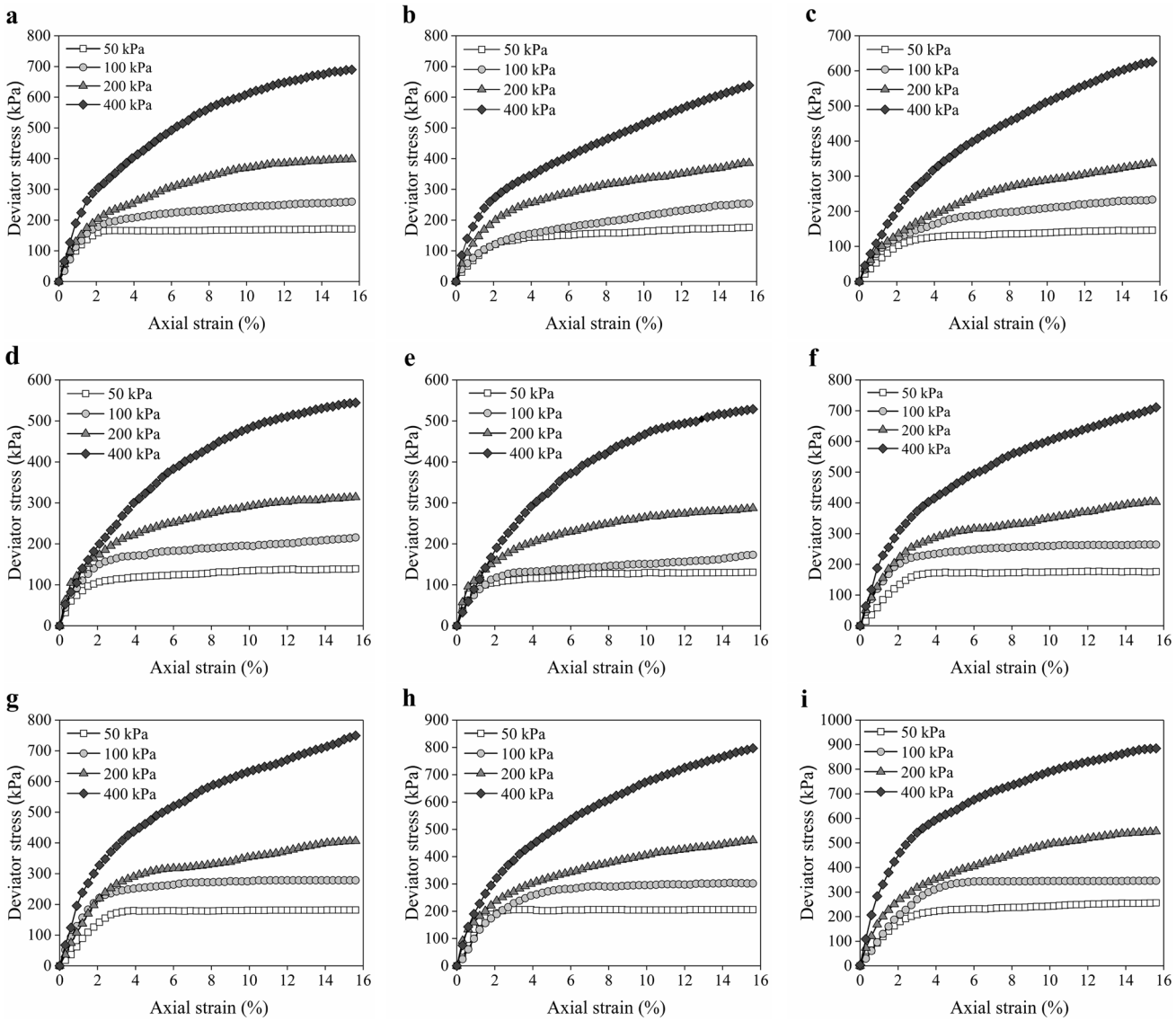

Fig. 5 Stress−strain curves of acid- and alkali-contaminated loess: **a** deionized water; **b** 0.5 M HCl; **c** 1 M HCl; **d** 2 M HCl; **e** 3.5 M HCl; **f** 0.5 M NaOH; **g** 1 M NaOH; **h** 2 M NaOH; **i** 3.5 M NaOH

solutions, the failure strength was notably reduced, and at lower concentrations (0.5 and 1 M), a certain attenuation occurred. However, this attenuation was relatively gentle, and with increasing concentration (2 and 3.5 M), the attenuation gradually increased. However, regarding the samples contaminated by NaOH, the failure strength was improved, but the trend was moderate. At a low concentration (0.5 and 1 M), the increase in the failure strength was small, while at moderate and high concentrations (2 and 3.5 M), the increment increased. Comparing Fig. 6a and b shows that at a low concentration, the failure strength of the soil was more sensitive to acid contamination, while at a higher concentration, the failure strength was more sensitive to alkaline contamination.

Shear strength parameters

Based on the Mohr−Coulomb criterion, the shear strength parameters, i.e., cohesion and friction angle, of the contaminated samples were determined, as depicted in Fig. 7. Apparently, the cohesion of the samples immersed in the hydrochloric acid solutions decreased, especially at a high concentration. In regard to the loess samples contaminated by 1 M HCl, the cohesion decreased by 5.85 kPa relative to the samples immersed in deionized water, and the relative loss (the difference divided by the initial value) reached 15.18%. After immersion in the high-concentration (3.5 M) HCl solution, compared to those of the samples immersed in deionized water, the cohesion decreased by 20.15 kPa,

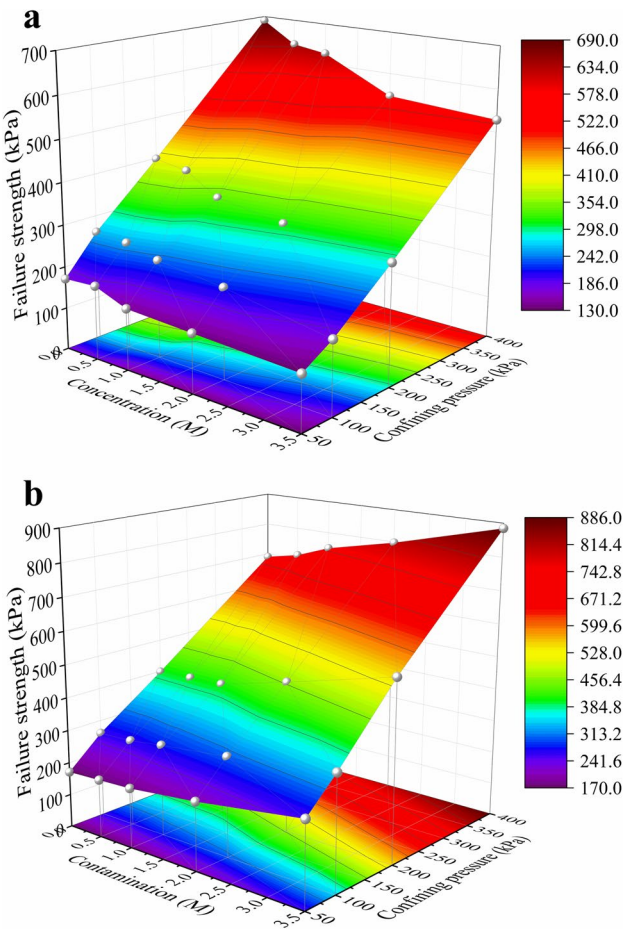

Fig. 6 Variation in failure strength of loess contaminated by acid and alkali: **a** HCl contamination; **b** NaOH contamination

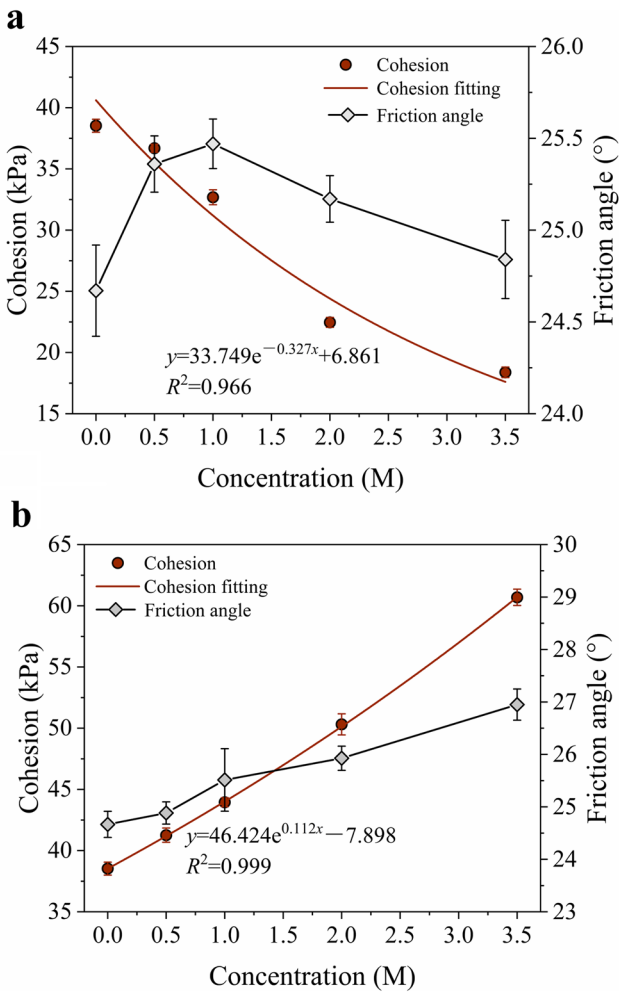

Fig. 7 Variation in shear strength parameters of loess contaminated by acid and alkali: **a** HCl contamination; **b** NaOH contamination

and the relative loss reached 52.30%. Nevertheless, regarding the samples immersed in the NaOH solutions, at a low concentration (1 M), the soil cohesion slightly increased, at an increment of 5.42 kPa, which represents an increase of 14.07% over the initial value. However, after immersion in the high-concentration (3.5 M) NaOH solution, compared to that of the samples immersed in the lower-concentration solution (2 M), the cohesion increased by 10.38 kPa, which represents an increase of 57.51% over the initial value (immersion in deionized water, 0 M). These data revealed that acid contamination imposed a deteriorating effect on the cohesion of natural loess, while alkali contamination exerted a promoting effect.

With increasing concentration of the HCl immersion solution, the friction angle initially increased slightly and then moderately decreased, but the overall change was less than 1°. Under NaOH immersion, with increasing concentration, the overall friction angle slightly increased, and the change range was larger than that obtained under HCl immersion, but the overall change remained less than 3°. Considering that the friction angle of the samples subjected to HCl and NaOH immersion fluctuated only slightly, the friction angle could be regarded as a secondary factor when assessing the mechanism of the influence on the soil shear strength.

Evolution of the soil microstructure

Particle structure characteristics

Figure 8 shows micrographs of the samples after immersion in deionized water and the 2 M HCl and NaOH solutions under 100, 3000, and 8000 times magnification. The microstructure of the intact loess mainly comprised four aspects, namely, the particle morphology, cementitious substance, interparticle association, and pore structure (Li et al. 2020a; Liu et al. 2015; Xu et al. 2018; Ye and Li 2019). After immersion in deionized water (Fig. 8a–c), the shapes of the soil particles were relatively intact, which is manifested as skeleton particles in the field of view (as indicated in the solid elliptical frame) with clear outlines, clean

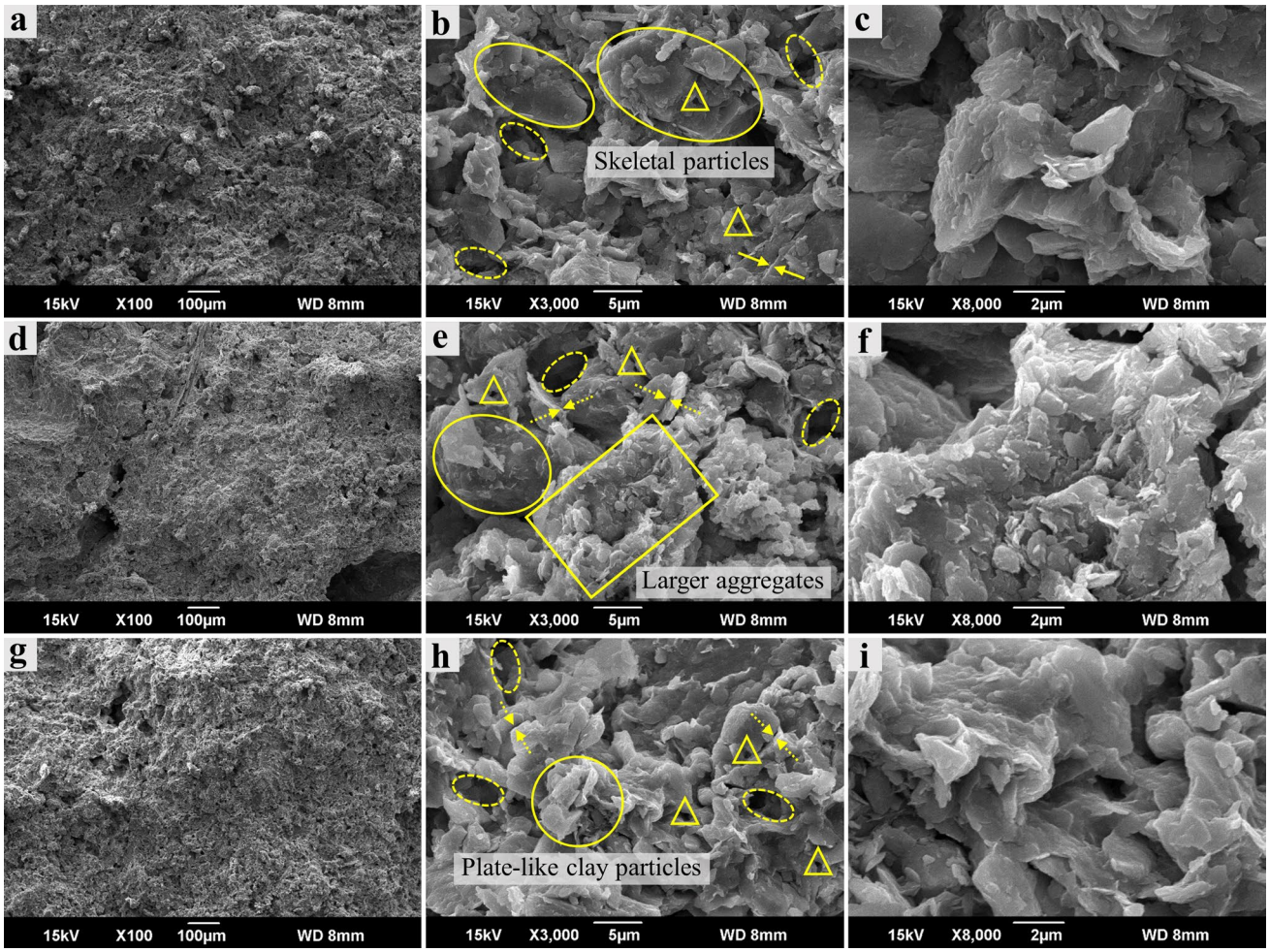

Fig. 8 SEM images of loess contaminated by acid and alkali at different magnifications: **a** deionized water at 100×; **b** deionized water at 3000×; **c** deionized water at 8000×; **d** 2 M HCl at 100×; **e** 2 M HCl at 3000×; **f** 2 M HCl at 8000×; **g** 2 M NaOH at 100×; **h** 2 M NaOH at 3000×; **i** 2 M NaOH at 8000×. Note: × means magnification

surfaces, and cementation between the abundant grains. The interparticle association mostly indicated notable face-to-face association (as shown by the pair of solid arrows), and the pores exhibited pronounced dual-porosity structures (as defined by Barden and Sides Geoffrey (1970)), namely, stent pores (mostly interaggregate pores, marked in the dashed elliptical frame) and mosaic pores (mostly intra-aggregate pores, marked in the triangular frame). The contact area of the pores was fragile (mostly edge-to-edge or edge-to-face association, as illustrated by the pair of dotted arrows).

Nevertheless, after exposure to water, the interparticle strength of the soil quickly decreased from the observed weak association, causing collapse. Based on Fig. 8d–f, after immersion in the 2 M HCl solution, the soil structure considerably deteriorated, a large quantity of cementation had dissolved, the original dense structure in the field of view loosened, and the edge-to-face association ratio between the grains increased. Moreover, a flocculation effect on the soil fabric occurred, which was manifested by the blurring of the boundary between the pores and particles in the field of view, and the surface of the skeleton particles became uneven due to breakage, resulting in a notable increase in the proportion of stent or mosaic pores. After immersion in the 2 M NaOH solution (Fig. 8g–i), the overall microstructure of the soil remained relatively intact, and comparing Fig. 8g and d shows that the density of the soil microstructure under NaOH immersion was higher than that under HCl immersion. Higher magnification (Fig. 8h–i) revealed that a small amount of the minerals had dissolved, and aggregates were dispersed. In addition, a new cementitious substance was observed on the original cemented interparticle surface, which filled the stent and mosaic pores, and the soil structure integrity remained high. This may occur due to the reaction of certain active minerals with NaOH to form new cementitious substances that offset local structural damage and enhance the bonding degree of the soil microstructure.

Pore structure characteristics

As shown in Fig. 9, the relationship between the pore distribution density and pore diameter of the HCl- and NaOH-contaminated samples exhibited a bimodal pore size distribution with a main peak and a subpeak. This typical bimodal pore size distribution has been found in mercury intrusion testing of various soils, including compacted clays, intact aggregated loams, residual soils, and sediments (Alonso et al. 2005; Anandarajah and Lavoie 2002; Li and Zhang 2009; Mallants et al. 1997).

Regarding the HCl-contaminated samples (Fig. 9a), with increasing concentration, both the main peak and subpeak slightly increased and shifted to the right. Notably, the volume and size of the soil pores had increased to various degrees after immersion in the HCl solutions of various concentrations. In regard to the samples immersed in the NaOH solutions (Fig. 9b), the main peak slightly decreased with a slight shift to the left, while the subpeak slightly increased with a slight shift to the left, and this trend became increasingly pronounced with increasing NaOH solution concentration. This indicated that after NaOH immersion, the volume and size of the larger soil pores decreased, the size of the smaller pores decreased, and the volume slightly increased.

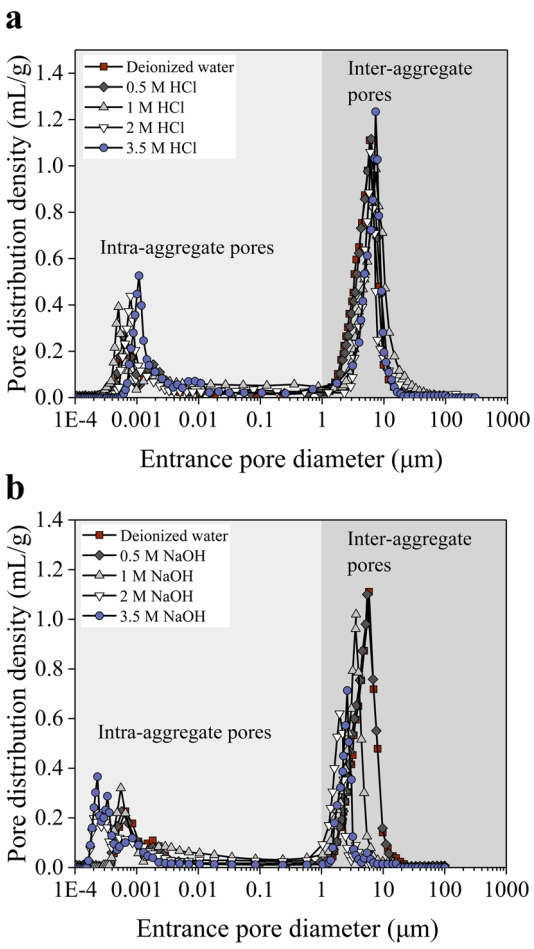

Fig. 9 Pore size distribution of loess contaminated by acid and alkali: **a** HCl contamination; **b** NaOH contamination

Interaggregate and intra-aggregate pores were clearly identified in the specimen at 3000 times magnification (Figs. 8b, e and h), and their representative diameters were estimated at approximately 1 and 5 μm, respectively. In Fig. 9, since all samples exhibited a similar distribution below 1 μm, the boundary between the interaggregate and intra-aggregate pores was considered 1 μm. With the use of the approach of combining the SEM and MIP results, the dual-porosity structure of various clays was quantified, such as intact and recompacted loess (Ng et al. 2016), lateritic clay (Ng et al. 2020a) and decomposed granitic soil (Li and Zhang 2009). Figure 9 shows that the volume and size of the interparticle and interaggregate pores increased under HCl contamination. In contrast, under NaOH contamination, the volume and size of the interaggregate pores decreased, while the size of the interaggregate pores decreased and the volume slightly increased.

Evolution of the chemical composition and Atterberg limits

Chemical composition

Table 2 presents the evolution of the insoluble salts and pore water pH of the samples contaminated with the HCl and NaOH solutions. After HCl immersion, except for CO_3^{2-} and HCO_3^-, the other soil ions increased to various degrees, especially Na^+, Ca^{2+}, Mg^{2+}, SO_4^{2-} and Cl^-, which were all markedly enhanced. However, the $CaCO_3$ content sharply decreased after immersion in an HCl solution, and the H^+ concentration in the soil pore water increased, demonstrating a notable reduction in the pH value. In contrast, under NaOH immersion, the changes in SO_4^{2-} and CO_3^{2-} in the soil were the most obvious. The former considerably increased, while the latter exhibited a slightly increasing trend, but the increase was much smaller than that in the former. The remaining anions notably declined. Regarding the cations, the more active Na^+, K^+, Ca^{2+} and Mg^{2+} all manifested a decreasing trend, while the less active Al^{3+} exhibited a slightly increasing trend. Under NaOH immersion, insoluble salt $CaCO_3$ increased. The pH value of the soil pore water also increased with increasing OH^- concentration.

Atterberg limits

Figure 10 shows the change in the Atterberg limits of the loess samples subjected to acid and alkali contamination conditions. After HCl contamination, the LL and PL values

Table 2 variations of sample chemical properties in acid or alkali contamination

Solution	Concentration (M)	Ion soluble (mg/L)										$CaCO_3$ (%)	PH value of pore Water
		Na^+	Ca^{2+}	Mg^{2+}	K^+	Al^{3+}	Fe^{3+}	SO_4^{2-}	CO2-3	HCO-3	Cl^-		
Deionized water	0	195.1	112.7	18.5	4.4	–	–	479.2	12.6	26.8	176.9	16.8	7.9
HCl	0.5	707.3	1239.6	125.7	16.3	–	13.8	871.7	4.8	21.8	1068.3	2.7	7.3
	1	1073.6	2139.6	198.4	29.4	–	21.5	1141.6	–	12.7	2197.9	–	6.5
	2	1470.2	3054.9	398.1	45.6	–	26.3	1642.2	–	6.7	4372.5	–	5.6
	3.5	1786.3	3829.5	518.6	67.4	–	18.6	2037.3	–	–	6881.2	–	4.9
NaOH	0.5	130.1	49.6	14.7	7.2	4.2	–	571.3	18.2	56.9	141.3	17.3	8.6
	1	89.4	26.8	8.3	6.5	6.6	–	686.9	26.3	227.2	97.5	21.8	9.3
	2	39.8	11.5	3.7	5.3	14.1	–	754.4	48.8	312.5	50.2	25.6	10.7
	3.5	18.3	5.9	–	4.9	19.7	–	785.6	66.4	386.1	17.2	34.1	11.6

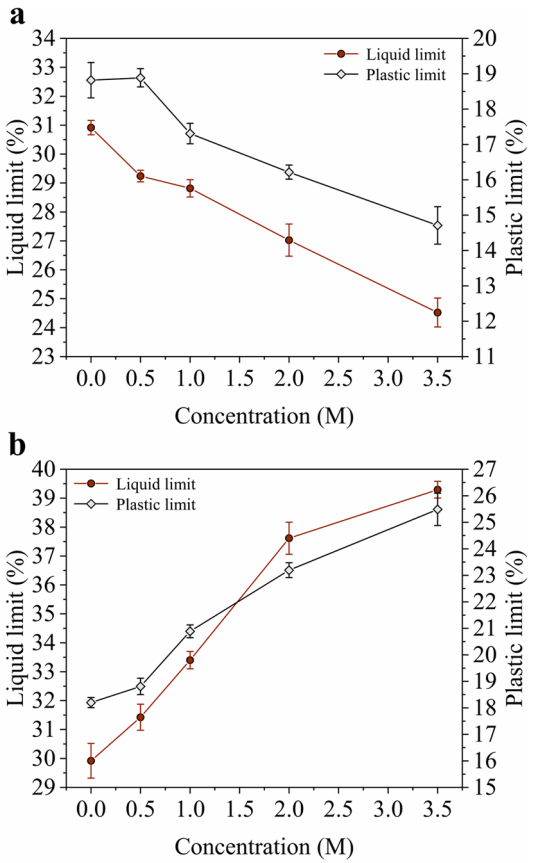

Fig. 10 Atterberg limits of loess contaminated by acid and alkali: **a** HCl contamination; **b** NaOH contamination

of the soil samples exhibited a negative trend, while after NaOH contamination, both exhibited a positive trend. As the HCl solution concentration was increased from the initial value to 3.5 M, the LL value of the soil specimens was reduced from 30.9 to 24.5%, which represents a loss of 20.71% from the initial level. Moreover, the observed reduction in the PL value was 4.1%, which represents a loss of 21.81% from the initial level (Fig. 10a). In contrast, when the NaOH immersion solution concentration was increased from the initial concentration to 3.5 M, the LL value of the specimens increased from 30.9 to 39.3%, while the observed increment in the PL value reached 6.7% (Fig. 10b). These data indicated that the Atterberg limits of the tested loess deteriorated after acid contamination but were improved after alkali contamination.

Discussion

Effect of acid contamination on the shear strength of intact loess

After the intact loess samples were immersed in the HCl solutions, a large amount of salt cement connecting the soil skeleton particles was dissolved, the integrity of the microstructure deteriorated (Fig. 8), the size and volume of the pores between the skeleton particles increased (Fig. 9), the cohesion was attenuated, and the stress−strain curves of the soil samples revealed a trend of maximum deviator stress attenuation (Figs. 5, 6). Natural loess is rich in various calcium salt substances (~ 10 to 15%) (Derbyshire 2001; Gao 1988; Zhang et al. 2018b), which are a crucial part of its cementitious strength. However, these substances were readily dissolved in the HCl solutions (Table 2), causing the originally firmly connected soil skeleton particles to loosen, thus reducing the initial cohesion. Moreover, this led to increases in the particle spacing, pore volume, and pore size, which directly caused a reduction in the connection between the particles and a decrease in the original cohesion. The MIP results indicated that the increase in loess porosity was particularly significant in the acidic environments. These processes resulted in rapid deterioration in the overall soil cohesion after HCl contamination. Indeed, the limitations of the MIP method should be assessed: (a) completely closed pores cannot be measured; (b) the ink-bottle effect occurs, i.e., pores with a large main body and a small mouth, similar to

the shape of ink bottles (formed by a complex pore network), can only be filled after reaching the intrusion pressure of the smallest pores (i.e., small constrictions or necks), resulting in some macropores not being detected; and c) the maximum applied pressure is insufficient for mercury to enter all intergranular pores (Ng et al. 2016; Xu et al. 2023). In this work, saturated samples were employed, and there were very few completely closed pores. Second, the obvious ink-bottle effect may lead to a conservative upper limit of the size and volume of the available pores, while it does not affect the variation trend in the pore size and volume of loess under acid and alkali contamination. Finally, the mercury injection pressure strictly followed the test standard of soil material (ASTM 2018), which could ensure that a large proportion of interlayer pores is captured, resulting in a slight influence on the test results.

In addition, after the samples were immersed in the HCl solutions, the pH value of the pore water declined (Table 2), and a large amount of H^+ displaced a certain amount of free Ca^{2+}, Na^+, Mg^{2+}, and K^+ (as indicated in Eqs. (3)–(8)), which were dispersed in the free and bound soil water. These ions came into contact with the DDLs of clay particles and caused a decrease in the surface potential, ion–dipole force and moisture absorption by clay (Duan et al. 2021; Fang et al. 2022; Xu et al. 2021), and combined with certain low-plasticity substances, water weakly bound to the clay surface was removed, the DDL thickness was reduced, and the soil plasticity decreased (Liu et al. 2021b; Sunil et al. 2006; Wu et al. 2021). Although this process slightly reduced the particle spacing, it notably contributed to soil structure damage (Fig. 8). The soil shear strength is controlled not only by the structural strength of the soil skeleton but also, to a large extent, by the DDL thickness. Since each soil particle is connected by DDLs, the overall performance is that of water bonding (Li et al. 2020b; Liu et al. 2015). The loss of water bonding definitely causes irreversible damage to the metastable structure or even the collapse of natural loess.

The friction angle is principally controlled by the soil density, gradation, mineral composition, and particle roughness (Wang et al. 2019; Xu et al. 2020; Zhang et al. 2018b). Since the gradation and roughness of natural loess particles are related to their deposition history (Liu et al. 2021c; Liu and Ding 1998), these quantities varied only slightly after HCl immersion. Most of the primary minerals do not dissolve in acid, and only a portion of the free oxides and insoluble salts may react (Sun et al. 2021). Thus, the overall decrease in the soil density was essentially limited. Therefore, the friction angle also slightly fluctuated. Similar findings were reported by Ghobadi et al. (2014), who considered that the stress−strain characteristics and undrained shear strength of Hamedan clay greatly deteriorated when the pH value of the soil pore water was lower than 3 and significantly increased when a pH value of 9 was reached. Notably, the soil grain size distribution, mineral composition and solution employed to adjust the pH value of the pore water in their samples were very consistent with those of our samples and solutions. In addition, several researchers reported findings that are consistent with ours (Lei et al. 2020; Spagnoli et al. 2012; Sun et al. 2021), whereas an increase in the shear strength was reported by Zhang et al. (2018a). They noted that the shear strength of natural loess soaked in oxalic and phosphoric acid (for 3 days) was improved. The authors mainly attributed this finding to their consolidation quick shear test scheme. When loess is soaked in an acid solution, the pores increase, and the soil structure relaxes. Under the same axial pressure, more weakly bound water is discharged, the spaces between the soil particles are reduced, and the soil skeleton becomes denser. These seemingly contradictory findings again confirm that an acidic environment imposes a notable deteriorating effect on the structure and shear strength of natural loess.

$$CaCO_3 + 2H^+ \rightarrow Ca^{2+} + H_2O + CO_2 \uparrow \quad (3)$$

$$MgO + 2H^+ \rightarrow Mg^{2+} + H_2O \quad (4)$$

$$Fe_2O_3 + 6H^+ \rightarrow 2Fe^{3+} + 3H_2O \quad (5)$$

$$Al_2O_3 + 6H^+ \rightarrow 2Al^{3+} + 3H_2O \quad (6)$$

$$K_2O + 2H^+ \rightarrow 2K^+ + H_2O \quad (7)$$

$$Na_2O + 2H^+ \rightarrow 2Na^+ + H_2O \quad (8)$$

Effect of alkali contamination on the shear strength of intact loess

Under NaOH immersion, the free oxides (Al_2O_3, SiO_2, etc.) in soil are sensitive to NaOH and can form Na_2SiO_3 and H_2SiO_3 colloids and $Al(OH)_3$ precipitates, as indicated in Eqs. (9)–(12) (Lei et al. 2020; Xu et al. 2021). First, these new viscous colloids or flocs flow together with fine particles due to Brownian motion and fill surrounding pores. After embedment and hardening, they form denser and firmer connections (Fig. 8), which causes a direct enhancement in the overall cohesion and interparticle friction of the soil matrix. Second, when immersed in a NaOH solution, the notable ion exchange effect yields a large amount of free Na^+, which readily penetrates and is absorbed by the DDLs of clay minerals (Sruthi and Reddy 2017). This facilitates the increase in the thermodynamic potential of the clay particle surface and promotes DDL thickening, which is also the reason for the slight expansion of the sample

volume after NaOH immersion. Moreover, NaOH can react with CO_2 to produce Na_2CO_3 (as indicated in Eq. (13)), and slight changes in the temperature and humidity produce water-rich compounds and result in a certain expansion pressure. Therefore, after NaOH immersion, the small amount of white crystals observed on the sample surface after contact with air may be $Na_2CO_3{\cdot}nH_2O$. In fact, when particles are locally eroded by alkali, their roughness and embedded friction are reduced, which partially counteracts the strengthening effect of the aforementioned interparticle friction. Nevertheless, the restraint of the external force during shearing enhanced the embedment and friction effects between the soil particles. This led to a limited increase in the friction angle of the samples under alkali contamination. This also indicated that under NaOH contamination, the potential reason for the improvement in the soil shear strength is that the amendment effect of the new structure is greater than the damage effect on the original structure. Similar behavior was observed for Xiashu loess by Sun et al. (2021), who reported that the newly formed insoluble substances under alkali contamination led to an increase in the density and a decrease in the void ratio. Comparable conclusions were drawn by Wang et al. (2020), who considered that NaOH contamination in red soil (rich in aluminum and iron) generated new spherical cemented salts, which causes shear strength increase. Furthermore, in this study, it was shown that the evolution patterns of the plasticity of the soil specimens under the effect of HCl and NaOH contamination were completely the opposite, i.e., a reduction under HCl contamination and an increase under NaOH contamination, as shown in Fig. 10. This led to an increase in the soil liquidity index under HCl immersion and a decrease under NaOH immersion at the same water content, which is consistent with the findings of Locat and Demers (1988), namely, the liquidity index of clayey soil is negatively correlated with the undrained shear strength.

$$SiO_2 + 2NaOH \rightarrow Na_2SiO_3 + H_2O \quad (9)$$

$$Na_2SiO_3 + CO_2 + H_2O \rightarrow H_2SiO_3 \downarrow + Na_2CO_3 \quad (10)$$

$$Al_2O_3 + 2NaOH \rightarrow 2NaAlO_2 + H_2O \quad (11)$$

$$2NaAlO_2 + CO_2 + 3H_2O \rightarrow 2Al(OH)_3 \downarrow + Na_2CO_3 \quad (12)$$

$$2NaOH + CO_2 \rightarrow Na_2CO_3 + H_2O \quad (13)$$

In summary, combined with the schematic diagram of the microstructure of natural loess in the different hydrochemical environments, as shown in Fig. 11, the mechanisms of the evolution of the shear strength of acid- and alkali-contaminated loess could be obtained. After soil immersion in the acid or alkali solutions, a series of physical–chemical-hydraulic processes are induced, such as mineral compounding, ion exchange, and variation in the particle and pore structures, which causes damage to the original loess structure but also yields a new structure. The overall effect of the above changes in the external water chemical environment is either degradation or enhancement in the shear strength of intact loess, depending on whether damage of the original structure or the formation of a new structure dominates, respectively. The results of this investigation could be applied in geotechnical engineering, geological engineering and agricultural–environmental engineering projects, including excavation and unloading of acid- and alkali-contaminated slopes in loess areas and reclamation and restoration of acid- and alkali-contaminated land.

Conclusions

In this study, triaxial shear tests, SEM experiments, MIP tests, chemical composition analysis and Atterberg limit determination tests of loess samples contaminated by acid (HCl) or alkali (NaOH) were conducted to assess the microscopic mechanisms of the evolution of the shear strength. The following key conclusions could be obtained:

(1) The shear properties of the HCl-contaminated loess samples notably worsened. Specifically, the stress−strain curves indicated softening, the failure strength deteriorated, and the cohesion exponentially decreased with increasing HCl solution concentration. After immersion in the 3.5 M HCl solution, the cohesion loss reached 52.30% from the initial level (after immersion in deionized water), and the friction angle changed statistically.
(2) The shear properties of the NaOH-contaminated loess samples were improved, which is manifested as an increase in the maximum deviator stress (failure strength) of the stress−strain curve. After immersion in the 3.5 M NaOH solution, the cohesion increased by 57.51% over the initial level, and the friction angle moderately increased.
(3) With increasing HCl concentration, cementitious substances were dissolved, and the boundaries between the particles and pores became increasingly blurred. However, under NaOH contamination, the stent pores in the loess samples locally collapsed, and new cementation filled the surrounding pores to balance this local damage.
(4) Under HCl contamination, CO_3^{2-} and HCO_3^- in the loess specimens decreased, Na^+, Ca^{2+}, Mg^{2+}, SO_4^{2-} and Cl^- all increased notably, the $CaCO_3$ content sharply decreased, the pH value of the pore water greatly

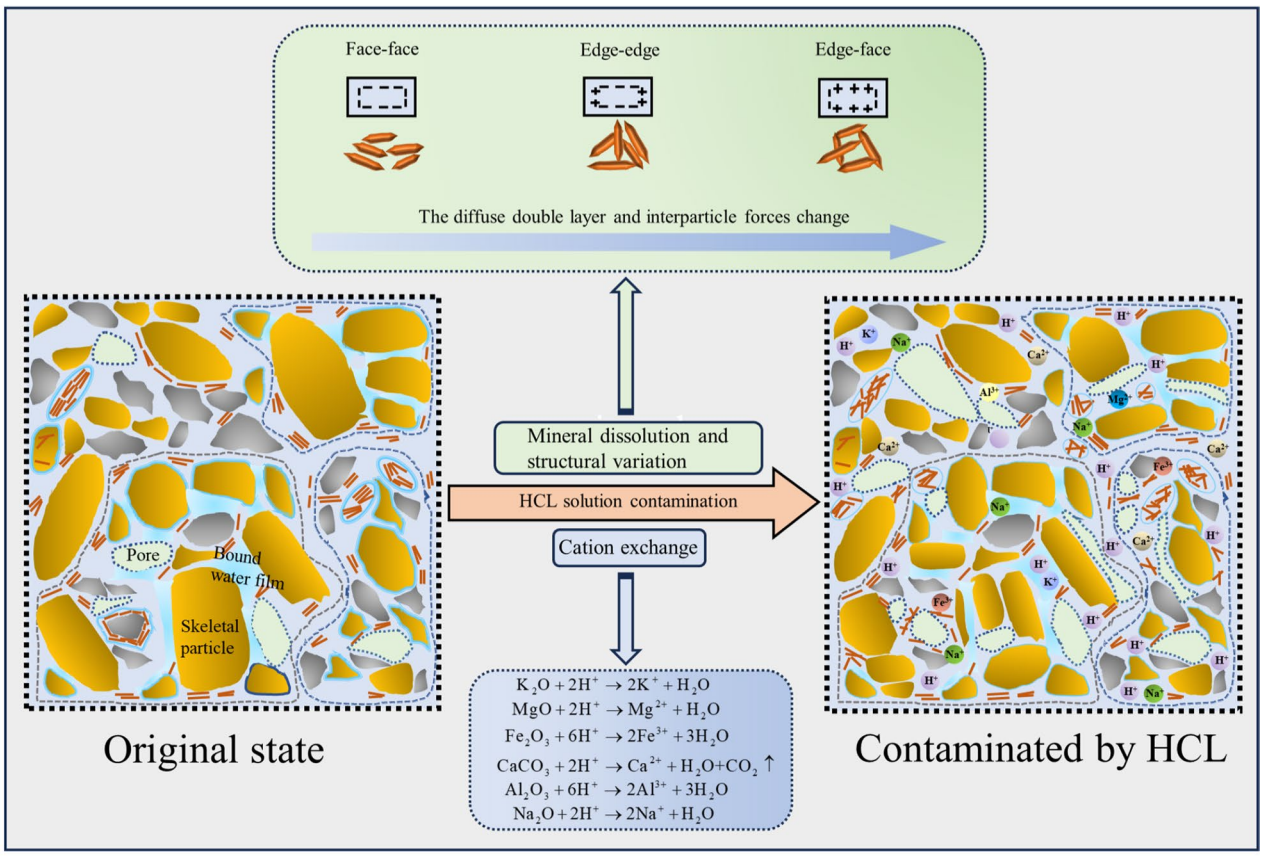

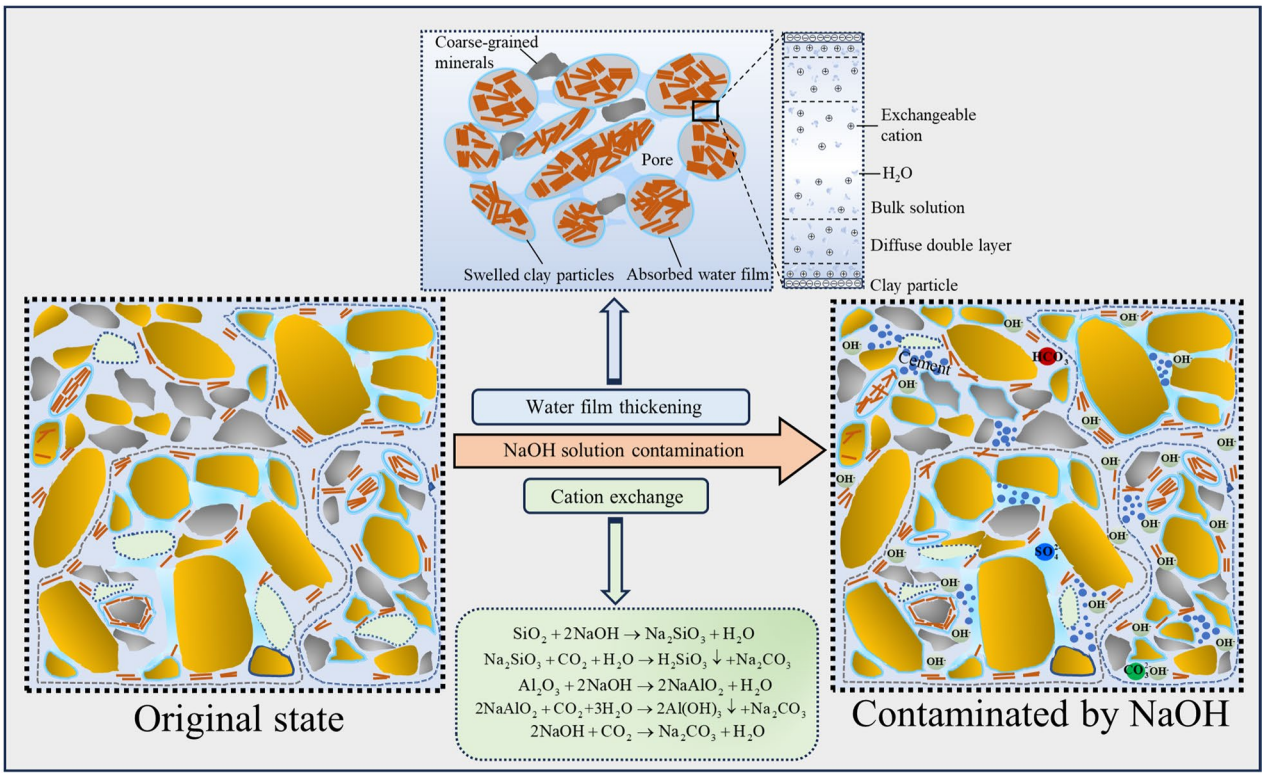

Fig. 11 Schematic diagram of the evolution of the microstructure of intact loess under acid and alkali contamination: **a** HCl contamination; **b** NaOH contamination

declined, and the Atterberg limits fell. Under NaOH contamination, the increase in SO_4^{2-} was considerable, followed by the increase in HCO_3^-, and the increase in CO_3^{2-} was slight. Na^+, K^+, Ca^{2+} and Mg^{2+} decreased, the pH value of the pore water remarkably increased, and the Atterberg limits increased.

(5) The structure of the loess samples varied (internal mineral dissolution, ion exchange, and pore and particle structure adjustment) during the evolution of the external aqueous chemical environment. Whether this variation involved degradation or strengthening depended on whether destruction of the original structure or growth of a new structure dominated, respectively.

These findings provide insight into the mechanisms of the variations in the shear behavior of intact loess due to contamination by acid and alkali solutions. This was only a preliminary study of the short-term or instantaneous mechanical behavior of acid- and alkali-contaminated loess. This motivates further research to investigate long-term changes in the strength, which may be closely related to the creep properties and rheological mechanism of soil.

Acknowledgements The authors thank the editor and four anonymous reviewers for their constructive comments, which greatly enhanced the quality of the manuscript.

Author contributions KL proposed the original idea; KL and WY designed the experiments; KL conducted the main tests and analyzed the data; WY and PL helped conduct the mechanical tests and analyzed the data; WY supported the project and discussed the results; KL prepared the manuscript. All authors have reviewed the manuscript.

Funding This work was supported by the National Natural Science Foundation of China (Grant No. 42072319) and the Postdoctoral Research Projects of Shaanxi Province, China (No. 2023BSHEDZZ309).

Data availability All the data related to the manuscript are reported within the paper and available from the corresponding author upon request.

Declarations

Conflict of interest The authors declare that they have no conflict of interest.

References

Abedi Koupai J, Fatahizadeh M, Mosaddeghi MR (2020) Effect of pore water pH on mechanical properties of clay soil. B Eng Geol Environ 79:1461–1469. https://doi.org/10.1007/s10064-019-01611-1

Alonso EE, Romero E, Hoffmann C, García-Escudero E (2005) Expansive bentonite–sand mixtures in cyclic controlled-suction drying and wetting. Eng Geol 81:213–226. https://doi.org/10.1016/j.enggeo.2005.06.009

Alonso EE, Pinyol NM, Gens A (2013) Compacted soil behaviour: initial state, structure and constitutive modelling. Géotechnique 63:463–478. https://doi.org/10.1680/geot.11.P.134

Anandarajah A, Lavoie D (2002) Numerical simulation of the microstructure and compression behavior of Eckernförde Bay sediments. Mar Geol 182:3–27. https://doi.org/10.1016/S0025-3227(01)00226-2

Anandarajah A, Zhao D (2000) Triaxial behavior of kaolinite in different pore fluids. J Geotech Geoenviron 126:148–156. https://doi.org/10.1061/(ASCE)1090-0241(2000)126:2(148)

ASTM (2011a) Standard practice for classification of soils for engineering purposes (USCS). ASTM D2487–11: West Conshohocken, PA

ASTM (2011b) Standard test method for consolidated undrained triaxial compression test for cohesive soils. ASTM D4767–11: West Conshohocken, PA

ASTM (2014) Standard practices for preserving and transporting soil samples. ASTM D4220M-14: West Conshohocken, PA

ASTM (2018) Standard test method for determination of pore volume and pore volume distribution of soil and rock by mercury intrusion porosimetry. ASTM D4404–18: West Conshohocken, PA

Bakhshipour Z, Asadi A, Huat BBK, Sridharan A, Kawasaki S (2016) Effect of acid rain on geotechnical properties of residual soils. Soils Found 56:1008–1020. https://doi.org/10.1016/j.sandf.2016.11.006

Barden L, Sides Geoffrey R (1970) Engineering behavior and structure of compacted clay. J Soil Mech Found Div 96:1171–1200. https://doi.org/10.1061/JSFEAQ.0001434

Bufflap SE, Allen HE (1995) Comparison of pore water sampling techniques for trace metals. Water Res 29:2051–2054. https://doi.org/10.1016/0043-1354(95)00032-G

Chavali RVP, Vindula SK, Reddy PHP, Babu A, Pillai RJ (2017) Swelling behavior of kaolinitic clays contaminated with alkali solutions: a micro-level study. Appl Clay Sci 135:575–582. https://doi.org/10.1016/j.clay.2016.10.045

Dai F, Lee CF, Wang S, Feng Y (1999) Stress–strain behaviour of a loosely compacted volcanic-derived soil and its significance to rainfall-induced fill slope failures. Eng Geol 53:359–370. https://doi.org/10.1016/S0013-7952(99)00016-2

Delage P, Audiguier M, Cui Y-J, Howat MD (1996) Microstructure of a compacted silt. Can Geotech J 33:150–158. https://doi.org/10.1139/t96-030

Derbyshire E (2001) Geological hazards in loess terrain, with particular reference to the loess regions of China. Earth-Sci Rev 54:231–260. https://doi.org/10.1016/S0012-8252(01)00050-2

Duan Z, Yan X, Sun Q, Tan X, Dong C (2021) Effects of water content and salt content on electrical resistivity of loess. Environ Earth Sci 80:469. https://doi.org/10.1007/s12665-021-09769-2

Eid HT, Al-Nohmi N, Wijewickreme D, Amarasinghe RS (2019) Drained peak and residual interface shear strengths of fine-grained soils for pipeline geotechnics. J Geotech Geoenviron 145:06019010. https://doi.org/10.1061/(ASCE)GT.1943-5606.0002131

Fang H, Ding X, Jiang C, Peng Y, Wang C (2022) Effects of layer thickness and temperature on desiccation cracking characteristics of coral clay. B Eng Geol Environ 81:391. https://doi.org/10.1007/s10064-022-02884-9

Gajo A, Maines M (2007) Mechanical effects of aqueous solutions of inorganic acids and bases on a natural active clay. Géotechnique 57:687–699. https://doi.org/10.1680/geot.2007.57.8.687

Gao G (1988) Formation and development of the structure of collapsing loess in China. Eng Geol 25:235–245. https://doi.org/10.1016/0013-7952(88)90029-4

Ghobadi MH, Abdilor Y, Babazadeh R (2014) Stabilization of clay soils using lime and effect of pH variations on shear strength

parameters. B Eng Geol Environ 73:611–619. https://doi.org/10.1007/s10064-013-0563-7
Graham RC (1999) X-Ray diffraction and the identification and analysis of clay minerals. Soil Sci 164:72–73. https://doi.org/10.1097/00010694-199901000-00011
Gratchev I, Towhata I (2013) Stress–strain characteristics of two natural soils subjected to long-term acidic contamination. Soils Found 53:469–476. https://doi.org/10.1016/j.sandf.2013.04.008
Gratchev Ivan B, Sassa K (2013) Cyclic shear strength of soil with different pore fluids. J Geotech Geoenviron 139:1817–1821. https://doi.org/10.1061/(ASCE)GT.1943-5606.0000901
Hu W, Cheng W-C, Wang L, Xue Z-F (2022) Micro-structural characteristics deterioration of intact loess under acid and saline solutions and resultant macro-mechanical properties. Soil till Res 220:105382. https://doi.org/10.1016/j.still.2022.105382
Husein Malkawi AI, Alawneh AS, Abu-Safaqah OT (1999) Effects of organic matter on the physical and the physicochemical properties of an illitic soil. Appl Clay Sci 14:257–278. https://doi.org/10.1016/S0169-1317(99)00003-4
Juang CH, Holtz RD (1986) A probabilistic permeability model and the pore size density function. Int J Numer Anal Met 10:543–553. https://doi.org/10.1002/nag.1610100506
Komine H, Watanabe Y (2010) The past, present and future of the geo-environment in Japan. Soils Found 50:977–982. https://doi.org/10.3208/sandf.50.977
Lei H, Wang L, Jia R, Jiang M, Zhang W, Li C (2020) Effects of chemical conditions on the engineering properties and microscopic characteristics of Tianjin dredged fill. Eng Geol 269:105548. https://doi.org/10.1016/j.enggeo.2020.105548
Li X, Zhang LM (2009) Characterization of dual-structure pore-size distribution of soil. Can Geotech J 46:129–141. https://doi.org/10.1139/T08-110
Li P, Xie W, Pak RYS, Vanapalli SK (2019a) Microstructural evolution of loess soils from the Loess Plateau of China. CATENA 173:276–288. https://doi.org/10.1016/j.catena.2018.10.006
Li X, Li L, Song Y, Hong B, Wang L, Sun J (2019b) Characterization of the mechanisms underlying loess collapsibility for land-creation project in Shaanxi Province, China—a study from a micro perspective. Eng Geol 249:77–88. https://doi.org/10.1016/j.enggeo.2018.12.024
Li X, Hong B, Wang L, Li L, Sun J (2020a) Microanisotropy and preferred orientation of grains and aggregates (POGA) of the Malan loess in Yan'an, China: a profile study. B Eng Geol Environ 79:1893–1907. https://doi.org/10.1007/s10064-019-01674-0
Li Y, Zhang W, He S, Aydin A (2020b) Wetting-driven formation of present-day loess structure. Geoderma 377:114564. https://doi.org/10.1016/j.geoderma.2020.114564
Li P, Sun Q, Geng J, Yan X, Tang L (2022) Radon exhalation from temperature treated loess. Sci Total Environ 832:154925. https://doi.org/10.1016/j.scitotenv.2022.154925
Lian B, Peng J, Zhan H, Wang X (2019) Mechanical response of root-reinforced loess with various water contents. Soil till Res 193:85–94. https://doi.org/10.1016/j.still.2019.05.025
Lian B, Peng J, Zhan H, Huang Q, Wang X, Hu S (2020a) Formation mechanism analysis of irrigation-induced retrogressive loess landslides. CATENA 195:104441. https://doi.org/10.1016/j.catena.2019.104441
Lian B, Wang X, Peng J, Huang Q (2020b) Shear rate effect on the residual strength characteristics of saturated loess in naturally drained ring shear tests. Nat Hazards Earth Syst Sci 20:2843–2856. https://doi.org/10.5194/nhess-20-2843-2020
Lian B, Wang X, Liu K, Hu S, Feng X (2021) A mechanical insight into the triggering mechanism of frequently occurred landslides along the contact between loess and red clay. Sci Rep 11:17556. https://doi.org/10.1038/s41598-021-96384-7
Lian B, Wang X, Zhan H, Wang J, Peng J, Gu T, Zhu R (2022) Creep mechanical and microstructural insights into the failure mechanism of loess landslides induced by dry-wet cycles in the Heifangtai platform. China Eng Geol 300:106589. https://doi.org/10.1016/j.enggeo.2022.106589
Liu T, Ding Z (1998) Chinese loess and the paleomonsoon. Annu Rev Earth Planet Sci 26:111–145. https://doi.org/10.1146/annurev.earth.26.1.111
Liu Z, Liu F, Ma F, Wang M, Bai X, Zheng Y, Yin H, Zhang G (2015) Collapsibility, composition, and microstructure of loess in China. Can Geotech J 53:673–686. https://doi.org/10.1139/cgj-2015-0285
Liu K, Hu W, Gao C, Ye W (2021a) Energy dissipation of an infinite damping beam supported by saturated poroelastic halfspace. Phys Scr 96:055220. https://doi.org/10.1088/1402-4896/abe9ef
Liu K, Ye W, Jing H (2021b) Shear strength and damage characteristics of compacted expansive soil subjected to wet–dry cycles: a multi-scale study. Arab J Geosci 14:2866. https://doi.org/10.1007/s12517-021-09260-z
Liu K, Ye W, Jing H (2021c) Shear strength and microstructure of intact loess subjected to freeze-thaw cycling. Adv Mater Sci Eng 2021:1173603. https://doi.org/10.1155/2021/1173603
Liu K, Ye W, Jing H (2023) Multiscale evaluation of the structural characteristics of intact loess subjected to wet/dry cycles. Nat Hazards. https://doi.org/10.1007/s11069-023-06253-x
Locat J, Demers D (1988) Viscosity, yield stress, remolded strength, and liquidity index relationships for sensitive clays. Can Geotech J 25:799–806. https://doi.org/10.1139/t88-088
Lu H, Xu S, Li D, Li J (2018) An experimental study of mineral and microstructure for undisturbed loess polluted by landfill leachate. KSCE J Civ Eng 22:4891–4900. https://doi.org/10.1007/s12205-017-1799-8
Ma J, Pan F, He J, Chen L, Fu S, Jia B (2012) Petroleum pollution and evolution of water quality in the Malian River Basin of the Longdong Loess Plateau, Northwestern China. Environ Earth Sci 66:1769–1782. https://doi.org/10.1007/s12665-011-1399-8
Ma J, Zhao X, Li S, Peng H, Xiao L, Ma D, Zhang X (2021) Exploring the clogging process in coarse soil deposits in a dam foundation. B Eng Geol Environ 81:16. https://doi.org/10.1007/s10064-021-02533-7
Mallants D, Mohanty BP, Vervoort A, Feyen J (1997) Spatial analysis of saturated hydraulic conductivity in a soil with macropores. Soil Technol 10:115–131. https://doi.org/10.1016/S0933-3630(96)00093-1
MCPRC (2009) Ministry of construction of the People's Republic of China: code for investigation of geotechnical engineering (GB50021–2001). China Architecture and Building Press, Beijing
Mitchell JK, Soga K (2007) Fundamentals of soil behavior, 3rd edn. Wiley, New York
MWPRC (2019) Ministry of water resources of the People's Republic of China: standard for geotechnical testing method (GB/T50123–2019). China Planning Press, Beijing
Nan J, Peng J, Zhu F, Ma P, Liu R, Leng Y, Meng Z (2021a) Shear behavior and microstructural variation in loess from the Yan'an area. China Eng Geol 280:105964. https://doi.org/10.1016/j.enggeo.2020.105964
Nan J, Peng J, Zhu F, Zhao J, Leng Y (2021b) Multiscale characteristics of the wetting deformation of Malan loess in the Yan'an area, China. J Mt Sci-Engl 18:1112–1130. https://doi.org/10.1007/s11629-020-6490-8
Ng CWW, Sadeghi H, Hossen SKB, Chiu CF, Alonso EE, Baghbanrezvan S (2016) Water retention and volumetric characteristics of intact and re-compacted loess. Can Geotech J 53:1258–1269. https://doi.org/10.1139/cgj-2015-0364
Ng CWW, Sadeghi H, Jafarzadeh F, Sadeghi M, Zhou C, Baghbanrezvan S (2019) Effect of microstructure on shear strength and

dilatancy of unsaturated loess at high suctions. Can Geotech J 57:221–235. https://doi.org/10.1139/cgj-2018-0592
Ng CWW, Akinniyi DB, Zhou C (2020a) Influence of structure on the compression and shear behaviour of a saturated lateritic clay. Acta Geotech 15:3433–3441. https://doi.org/10.1007/s11440-020-00981-1
Ng CWW, Owusu ST, Zhou C, Chiu ACF (2020b) Effects of sesquioxide content on stress-dependent water retention behaviour of weathered soils. Eng Geol 266:105455. https://doi.org/10.1016/j.enggeo.2019.105455
Pécsi M (1990) Loess is not just the accumulation of dust. Quatern Int 7–8:1–21. https://doi.org/10.1016/1040-6182(90)90034-2
Penumadu D, Dean J (2000) Compressibility effect in evaluating the pore-size distribution of kaolin clay using mercury intrusion porosimetry. Can Geotech J 37:393–405. https://doi.org/10.1139/t99-121
Ratnaweera P, Meegoda J (2006) Shear strength and stress-strain behavior of contaminated soils. Geotech Test J 29:133–140. https://doi.org/10.1520/GTJ12686
Rogers CDF, Dijkstra TA, Smalley IJ (1994) Hydroconsolidation and subsidence of loess: studies from China, Russia, North America and Europe—in memory of Jan Sajgalik. Eng Geol 37:83–113. https://doi.org/10.1016/0013-7952(94)90045-0
Romero E (1999) Characterisation and thermo-hydro-mechanical behaviour of unsaturated Boom clay: an experimental study. PhD dissertation Universitat Politècnica de Catalunya: Spain. https://doi.org/10.1520/D0422-63R07E02
Shen Y, Lv Y, Yang H, Ma W, Zhang L, Wei X (2022) Pore development and mechanical properties of iced concrete during hydration. Constr Build Mater 353:129077. https://doi.org/10.1016/j.conbuildmat.2022.129077
Spagnoli G, Rubinos D, Stanjek H, Fernández-Steeger T, Feinendegen M, Azzam R (2012) Undrained shear strength of clays as modified by pH variations. B Eng Geol Environ 71:135–148. https://doi.org/10.1007/s10064-011-0372-9
Sruthi PL, Reddy PHP (2017) Characterization of kaolinitic clays subjected to alkali contamination. Appl Clay Sci 146:535–547. https://doi.org/10.1016/j.clay.2017.07.012
Stoltz G, Cuisinier O, Masrouri F (2012) Multi-scale analysis of the swelling and shrinkage of a lime-treated expansive clayey soil. Appl Clay Sci 61:44–51. https://doi.org/10.1016/j.clay.2012.04.001
Sun S, Wang W, Wei J, Song J, Yu Y, He W, Zhang J (2021) The physical–mechanical properties degradation mechanism and microstructure response of acid–alkali-contaminated Xiashu loess. Nat Hazards 106:2845–2861. https://doi.org/10.1007/s11069-021-04570-7
Sunil BM, Nayak S, Shrihari S (2006) Effect of pH on the geotechnical properties of laterite. Eng Geol 85:197–203. https://doi.org/10.1016/j.enggeo.2005.09.039
Tan T, Huat BBK, Anggraini V, Shukla SK, Nahazanan H (2021) Strength behavior of fly ash-stabilized soil reinforced with coir fibers in alkaline environment. Journal of Natural Fibers 18:1556–1569. https://doi.org/10.1080/15440478.2019.1691701
Tiwari B, Tuladhar Gyanu R, Marui H (2005) Variation in residual shear strength of the soil with the salinity of pore Fluid. J Geotech Geoenviron 131:1445–1456. https://doi.org/10.1061/(ASCE)1090-0241(2005)131:12(1445)
Wang YH, Siu WK (2006) Structure characteristics and mechanical properties of kaolinite soils. I. Surface charges and structural characterizations. Can Geotech J 43:587–600. https://doi.org/10.1139/t06-026
Wang S, Ding J, Xu J, Ren J, Yang Y (2019) Shear strength behavior of coarse-grained saline soils after freeze-thaw. KSCE J Civ Eng 23:2437–2452. https://doi.org/10.1007/s12205-019-0197-9
Wang Q, Chen J, Liu J, Yu M, Geng W, Wang P, Wu Z (2020) Relationships between shear strength parameters and microstructure of alkaline-contaminated red clay. Environ Sci Pollut Res 27:33848–33862. https://doi.org/10.1007/s11356-020-09637-9
Wang J, Fan C, Zhang Y, Li Z (2022) Gully head activity and its influencing factors in China's Loess Plateau. J Soils Sediments 22:1792–1803. https://doi.org/10.1007/s11368-022-03182-3
Wang Q, Yan X, Dong Y, Su W, Meng Y, Sun W (2023) Effect of Beishan groundwater salinity on the self-sealing performance of compacted GMZ bentonite. Environ Earth Sci 82:391. https://doi.org/10.1007/s12665-023-11082-z
Washburn EW (1921) Note on a method of determining the distribution of pore sizes in a porous material. P Natl Acad Sci USA 7:115–116. https://doi.org/10.1073/pnas.7.4.115
Wen B, Yan Y (2014) Influence of structure on shear characteristics of the unsaturated loess in Lanzhou, China. Eng Geol 168:46–58. https://doi.org/10.1016/j.enggeo.2013.10.023
Wu Z, Deng Y, Chen Y, Gao Y, Zha F (2021) Long-term desalination leaching effect on compression/swelling behaviour of Lianyungang marine soft clays. B Eng Geol Environ 80:8099–8107. https://doi.org/10.1007/s10064-021-02414-z
Xu L, Coop MR, Zhang M, Wang G (2018) The mechanics of a saturated silty loess and implications for landslides. Eng Geol 236:29–42. https://doi.org/10.1016/j.enggeo.2017.02.021
Xu J, Li Y, Ren C, Lan W (2020) Damage of saline intact loess after dry-wet and its interpretation based on SEM and NMR. Soils Found 60:911–928. https://doi.org/10.1016/j.sandf.2020.06.006
Xu P, Qian H, Zhang Q, Zheng L (2021) Exploring the saturated permeability of remolded loess under inorganic salt solution seepage. Eng Geol 294:106354. https://doi.org/10.1016/j.enggeo.2021.106354
Xu P, Qian H, Chen J, Wang L, Abliz X, He X, Ma G, Liu Y (2023) New insights into microstructure evolution mechanism of compacted loess and its engineering implications. B Eng Geol Environ 82:36. https://doi.org/10.1007/s10064-022-03058-3
Yan X, Duan Z, Sun Q (2021) Influences of water and salt contents on the thermal conductivity of loess. Environ Earth Sci 80:52. https://doi.org/10.1007/s12665-020-09335-2
Ye WJ, Li CQ (2019) The consequences of changes in the structure of loess as a result of cyclic freezing and thawing. B Eng Geol Environ 78:2125–2138. https://doi.org/10.1007/s10064-018-1252-3
Yu H, Sun D, Tian H (2019) NMR-based analysis of shear strength of weakly expansive clay in sodium chloride solution. Magn Reson Imaging 58:6–13. https://doi.org/10.1016/j.mri.2019.01.002
Zhang Y, Hu Z, Chen H, Xue T (2018a) Experimental investigation of the behavior of collapsible loess treated with the acid-addition pre-soaking method. KSCE J Civ Eng 22:4373–4384. https://doi.org/10.1007/s12205-017-0170-4
Zhang Y, Hu Z, Li L, Xue Z (2018b) Improving the structure and mechanical properties of loess by acid solutions: an experimental study. Eng Geol 244:132–145. https://doi.org/10.1016/j.enggeo.2018.07.023
Zhang S, Liu H, Chen W, Liu F (2020) Strength of recompacted loess affected by coupling between acid-base pollution and freeze-thaw cycles. J Cold Reg Eng 34:04020024. https://doi.org/10.1061/(asce)cr.1943-5495.0000230
Zhu J, Zhang H, Yang S, Wang T, Zhou G (2022) Physico-mechanical properties of loess-paleosol sequence from Q4 to Q1 strata in the Chinese Loess Plateau. B Eng Geol Environ 81:416. https://doi.org/10.1007/s10064-022-02899-2
Zhu C, Peng S, Li Z, Xu J, Deng G, Wang S (2023) Evaluation on wetting effect of loess high-fill embankment under rainfall and groundwater uplift. Transp Geotech 38:100916. https://doi.org/10.1016/j.trgeo.2022.100916